



## OPEN ACCESS

## EDITED BY

Zhanjun Guo,  
Fourth Hospital of Hebei Medical University,  
China

## REVIEWED BY

Zhibo Yan,  
Shandong University, China  
Chen Yang,  
Fudan University, China  
Chuanpeng Dong,  
Yale University, United States

## \*CORRESPONDENCE

Jun Wang

✉ Wangjundocor@aliyun.com

Xi Yan

✉ yxdoctor986@163.com

<sup>†</sup>These authors have contributed equally to this work.

## SPECIALTY SECTION

This article was submitted to Surgical Oncology, a section of the journal *Frontiers in Surgery*

RECEIVED 03 November 2022

ACCEPTED 02 March 2023

PUBLISHED 31 March 2023

## CITATION

Wu L-H, Wang X-X, Wang Y, Wei J, Liang Z-R, Yan X and Wang J (2023) Construction and validation of a prognosis signature based on the immune microenvironment in gastric cancer. *Front. Surg.* 10:1088292. doi: 10.3389/fsurg.2023.1088292

## COPYRIGHT

© 2023 Wu, Wang, Wang, Wei, Liang, Yan and Wang. This is an open-access article distributed under the terms of the [Creative Commons Attribution License \(CC BY\)](https://creativecommons.org/licenses/by/4.0/). The use, distribution or reproduction in other forums is permitted, provided the original author(s) and the copyright owner(s) are credited and that the original publication in this journal is cited, in accordance with accepted academic practice. No use, distribution or reproduction is permitted which does not comply with these terms.

# Construction and validation of a prognosis signature based on the immune microenvironment in gastric cancer

Li-Hong Wu<sup>1†</sup>, Xiang-Xu Wang<sup>2†</sup>, Yan Wang<sup>1</sup>, Jing Wei<sup>1</sup>,  
Zi-Rong Liang<sup>1</sup>, Xi Yan<sup>1\*</sup> and Jun Wang<sup>1\*</sup>

<sup>1</sup>Xijing 986 Hospital Department, Fourth Military Medical University, Xi'an, China, <sup>2</sup>Xijing Hospital, Fourth Military Medical University, Xi'an, China

**Background:** Gastric cancer (GC) is an aggressive malignant tumor with a high degree of heterogeneity, and its immune microenvironment is closely associated with tumor growth, development and drug resistance. Therefore, a classification system of gastric cancer based explicitly on the immune microenvironment context might enrich the strategy for gastric cancer prognosis and therapy.

**Methods:** A total of 668 GC patients were collected from TCGA-STAD ( $n = 350$ ), GSE15459 ( $n = 192$ ), GSE57303 ( $n = 70$ ) and GSE34942 ( $n = 56$ ) datasets. Three immune-related subtypes (immunity-H, -M, and -L) were identified by hierarchical cluster analysis based on the ssGSEA score of 29 immune microenvironment-related gene sets. The immune microenvironment-related prognosis signature (IMPS) was constructed via univariate Cox regression, Lasso-Cox regression and multivariate Cox regression, and nomogram model combining IMPS and clinical variables was further constructed by the "rms" package. RT-PCR was applied to validate the expression of 7 IMPS genes between two human GC cell lines (AGS and MKN45) and one normal gastric epithelial cell line (GES-1).

**Results:** The patients classified as immunity-H subtype exhibited highly expressed immune checkpoint and HLA-related genes, with enriched naïve B cells, M1 macrophages and CD8 T cells. We further constructed and validated a 7-gene (CTLA4, CLDN6, EMB, GPR15, ENTPD2, VWF and AKR1B1) prognosis signature, termed as IMPS. The patients with higher IMPS expression were more likely to be associated with higher pathology grade, more advanced TNM stages, higher T and N stage, and higher ratio of death. In addition, the prediction values of the combined nomogram in predicting 1-year (AUC = 0.750), 3-year (AUC = 0.764) and 5-year (AUC = 0.802) OS was higher than IMPS and individual clinical characteristics.

**Conclusions:** The IMPS is a novel prognosis signature associated with the immune microenvironment and clinical characteristics. The IMPS and the combined nomogram model provide a relatively reliable predictive index for predicting the survival outcomes of gastric cancer.

## KEYWORDS

immune microenvironment, gastric cancer, ssGSEA analysis, nomogram, prognosis signature

## 1. Introduction

Gastric cancer (GC) is a disease with considerable heterogeneity (1), and is the fourth most fatal cancer worldwide (2). Patients with GC are rarely diagnosed at an early stage owing to insidious symptoms, and 25%–50% of patients with late-stage GC eventually emerge metastasis during the disease (3). The heterogeneity of the tumor microenvironment has been reported as a potential biomarker of various cancer prognoses (4, 5). It is worth noting that the tumor microenvironment (TME) components play a crucial role in tumor development. Therefore, the identification of tumor immunophenotypes might provide new insights for understanding tumor biology and cancer prognosis.

With the development of bioinformatics technology, the immune microenvironment components can be quantitatively analyzed (6). The single-sample gene set enrichment analysis (ssGSEA) (7) has been used to calculate quantitative scores for different types of immune genomics characteristics and to further classify the different immunophenotypes. In the present study, we identified three immunophenotypes (immunity-H, -M and -L) based on the characteristics of 29 immune-related gene sets. In addition, we constructed an immune microenvironment-related prognosis signature (IMPS) *via* univariate Cox regression, Lasso-Cox regression, and multivariate Cox regression, and validated the model in testing and independent cohorts. The patients with higher IMPS were associated with higher grade, advanced TNM stages, higher T and N stage, and death. We further constructed a nomogram model combining IMPS and clinical variables. The IMPS and the combined nomogram model have potential value in predicting survival outcomes of gastric cancer.

## 2. Materials and methods

### 2.1. Data obtaining and processing

A total of 668 GC patients were collected from TCGA-STAD ( $n = 350$ ), GSE15459 ( $n = 192$ ), GSE57303 ( $n = 70$ ) and GSE34942 ( $n = 56$ ) datasets. The transcriptome data (HTSeq-FPKM) and clinical information were downloaded from <https://www.ncbi.nlm.nih.gov/geo/> and <https://portal.gdc.cancer.gov/>. The “limma” package was applied to perform deduplication and  $\log_2(x + 1)$  normalization processing on gene expression data (8).

### 2.2. Identification of three immune subtypes by hierarchical clustering analysis

The 29 immune microenvironment-related gene sets were collected from published literature (9). The ssGSEA algorithm *via* “GSVA” package was applied to evaluate the enrichment score of immunological characteristics in each GC sample (10).

### 2.3. Calculation of tumor purity and immune cell subpopulations

The package “ESTIMATE” was used to evaluate the stromal and immune cell components in the malignant tumor tissue to further estimate the total immune matrix scores, namely the Immune-, Stromal-, Estimate-scores, and to further evaluate the tumor purity (11). The subpopulations of 22 human immune cells were estimated by the relative subpopulations of RNA transcripts for cell type identification (CIBERORT) (12).

### 2.4. Screen of differentially expressed genes (DEGs) and function enrichment analysis

The DEGs between immunity-H and -L subtypes were screened *via* “limma” package with the screening conditions:  $|\log FC| > 1$ ,  $P < 0.05$  (13). The heatmap and volcano map were depicted to present the differentially expressed genes, and the GO enrichment circle diagrams performed *via* the “GOplot” R package were used to present the functional enrichment analysis of DEGs (14).

### 2.5. Construction and validation of the immune microenvironment-related prognosis signature (IMPS)

The 350 GC samples in the TCGA-STAD cohort were randomly divided into TCGA-training ( $n = 246$ ) and TCGA-testing cohorts ( $n = 104$ ) *via* the “cart” package with a ratio of 7:3 (15). The GSE15459 ( $n = 193$ ) and GSE57303 ( $n = 70$ ) cohorts were used as independent validations. In the TCGA-training cohort, we first screened the prognostic-related genes by univariate Cox regression ( $P < 0.05$ ), and further eliminate the collinearity among genes by Lasso-Cox regression analysis (16). Finally, we constructed a 7-gene prognosis signature *via* multivariate Cox analysis with the “stepwise regression method” (17). The IMPS of GC prognosis was calculated by the following formula:  $IMPS = -0.53 * CTLA4 + 0.12 * CLDN6 + 0.18 * EMB + 0.2 * GPR15 - 0.14 * ENTPD2 + 0.22 * VWF + 0.25 * AKR1B1$ . The prognosis value of these 7 hub genes and the IMPS were further validated in both TCGA-testing and GSE15459 cohorts.

### 2.6. Prediction value of IMPS in immunotherapy response

Due to the lack of clinical studies on gastric cancer immunotherapy including mRNA sequencing data, we used the IMvigor210 cohort (18) (metastatic urothelial carcinoma) and Riaz-2017 cohort (19) (advanced melanoma) to verify the potential predictive value of IMPS in the outcome of immunotherapy response.

## 2.7. Quantitative real-time PCR

Two human GC cell lines (AGS and MKN45) and one normal gastric epithelial cell line (GES-1) were cultured for testing the expression of 7 IMPS genes. In addition, we further performed the qPCR verification of seven Hub genes in five benign and five GC tissue samples. TRIzol (Servicebio, China) and PrimerScript™ RT Reagent kit (Takara, Tokyo, Japan) were used to extract total RNA and to further create the cDNA. The Real-Time PCR was performed by SYBR Green with the Real-Time PCR System (Roche, USA). The primers of the 7 hub genes were listed in [Table 1](#). Finally, the RNA expression was normalized to GAPDH.

## 2.8. Construction and evaluation of the combined nomogram considering IMPS and clinical characteristics

The combined nomogram prognostic model was constructed by the “rms” package based on clinical characteristics and the IMPS (20). The clinical characteristics included age, gender, pathology grade and TNM stage. The performance of the combined nomogram was evaluated by calibration plot using bootstrap method (21). And the time-ROC curve was performed to compare the prediction value among the combined nomogram model, IMPS, and clinical characteristics.

## 2.9. Statistical analyses

All statistical analyses were performed with the R software (version 4.1.2). The Mann–Whitney *U* test was used to compare the distribution difference of immune cells among different immune subtypes (22). The Chi-Squared test was used to evaluate the balance of clinical baseline between the training and testing cohorts (23). The Log-Rank test was performed to assess the differences in overall survival between different subtypes. The two-sided test with *P*-value <0.05 was considered statistically significant.

TABLE 1 Primer sequences of 7 hub genes.

Hub genes	Primer sequences
CTLA4(human)-F	GCCCTGCAGCTCTCCTGTTTT
CTLA4(human)-R	GGTTGCCGCACAGACTTCA
ENTPD2(human)-F	AGACAAGGAGAACGACACAGG
ENTPD2(human)-R	AGGCATCCAACAAGACTCTGG
CLDN6(human)-F	TGTTTCGGCTTGCTGGTCTAC
CLDN6(human)-R	CGGGGATTAGCGTCAGGAC
EMB (human)-F	CTGAGGGAGCAGTCTCCACG
EMB (human)-R	TGTAAGGCGGAATCTGGGGC
GPR15(human)-F	TTACTATGTACTACGAGCCAAACT
GPR15(human)-R	CTCCATGAGAACAAGGTTCC
VWF (human)-F	CCGATGCAGCCTTTTCGGA
VWF (human)-R	TCCCAAGATACACGGAGAGG
AKR1B1(human)-F	CTGGTGGATGAAGGGCTGG
AKR1B1(human)-R	GGGTGGCACTCAATCTGGTT

## 3. Results

### 3.1. Identification of three immune subtypes based on the ssGSEA score of 29 immune-related gene sets

We first identified three immune subtypes [immunity-H (*n* = 53, 15.1%), immunity-M (*n* = 248, 70.9%) and immunity-L (*n* = 49, 14.0%)] based on the ssGSEA score of 29 immune-related gene sets by the unsupervised clustering analysis. The heatmap showed that the immunity-H subtype has the highest enrichment score of immune-related genes ssGSEA than the immunity-L and -M subtypes ([Figure 1A](#)). The stromal, immune, and total stromal immune score in the immunity-H subtype were significantly higher than the immunity-M and -L subtypes ([Figures 1B–D](#), all *P* < 0.001), while tumor purity showed an opposite trend ([Figure 1E](#), *P* < 0.001). This indicates that the immunity-H GC subtype was associated with the highest infiltration of immune and stromal cells.

We further evaluated the infiltration fraction of 22 immune cells in GC samples by the “CIBERORT algorithm”. The results showed that patients in the immunity-H subtype had the higher fraction of memory B cells, resting dendritic cells, M1 macrophages, resting mast cells, plasma cells, activated CD4<sup>+</sup> memory T cells, CD8<sup>+</sup> T cells, and helper T cells than those classified as immunity-L subtype, while lower fraction of M0 macrophages, M2 macrophages and CD4<sup>+</sup> memory T cells ([Figure 1F](#), all *P* < 0.05). This indicates that the immunity-H GC subtype is dominated by immune positive cells, while the immunity-L subtype is dominated by immune negative cells.

### 3.2. The distribution of clinical characteristics among three immune subtypes

The immunity-H subtype had a relatively large proportion of people over 80 years of age ([Supplementary Figure S1A](#), immunity-H, 8%; immunity-M, 6%; immunity-L, 2%), and higher proportion of gastric corpus tumors ([Supplementary Figure S1D](#), immunity-H, 31%; immunity-L, 24%; immunity-L, 18%), higher proportions of pathological grade 3 ([Supplementary Figure S1E](#), immunity-H, 88%; immunity-M, 56%; immunity-L, 43%). The immunity-H subtype also had higher proportions of diffuse gastric adenocarcinoma ([Supplementary Figure S1F](#), immunity-H, 31%; immunity-M, 16%; immunity-L, 6%), but lower proportion of signet ring cell carcinoma ([Supplementary Figure S1F](#), immunity-H, 13%; immunity-M, 17%; immunity-L, 33%). In addition, patients with advanced TNM stage (stage III/IV) are more likely to present high immunity status ([Supplementary Figure S1G](#), immunity-H, 64%; immunity-M, 54%; immunity-L, 41%). Similar results were found in T stage3–4 ([Supplementary Figure S1H](#), immunity-H, 81%; immunity-M, 73%; immunity-L, 67%) and N stage2–3 ([Supplementary Figure S1I](#), immunity-H, 46%; immunity-M,

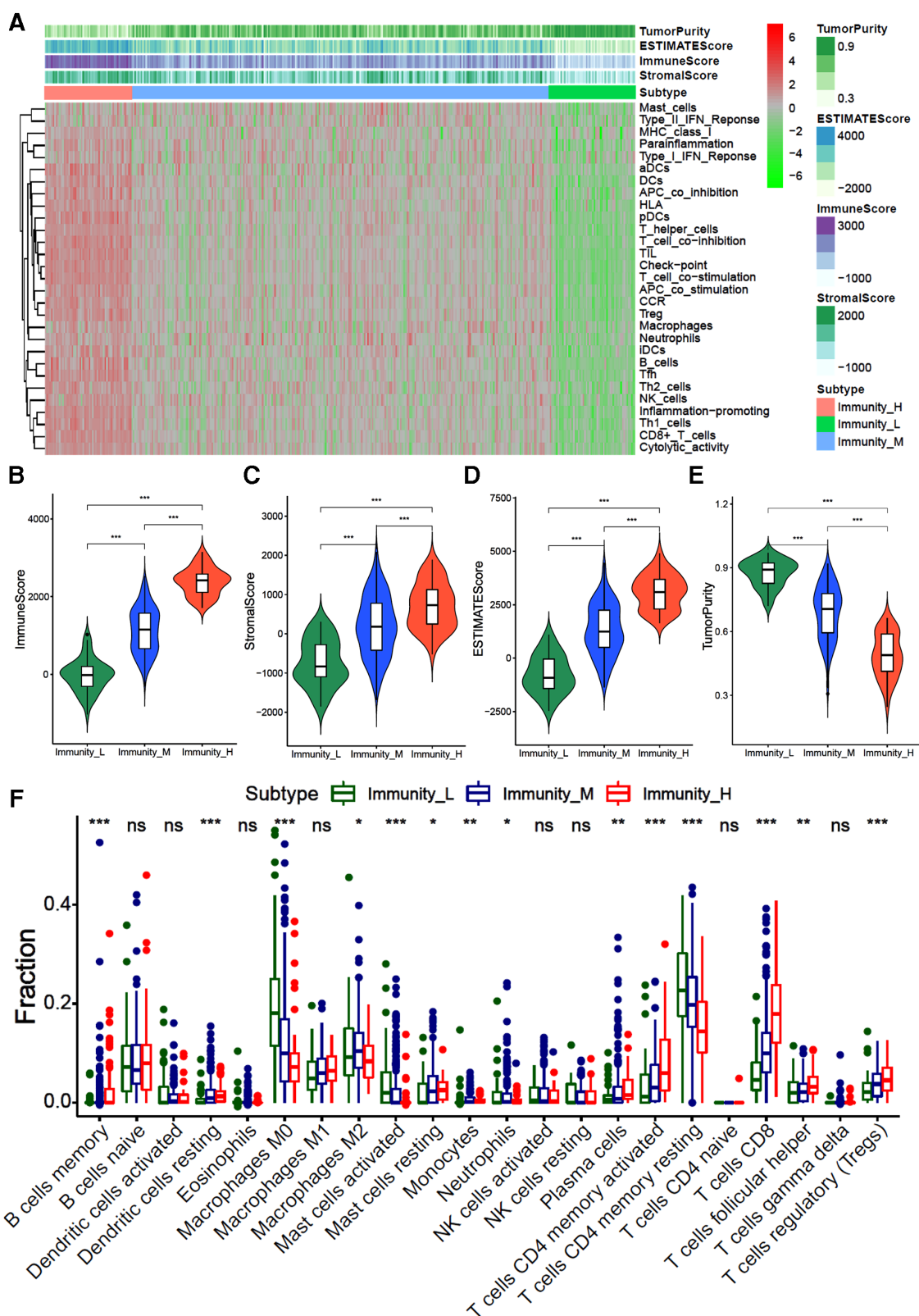


**FIGURE 1** Hierarchical cluster analysis of gastric cancer based on 29 immune-related gene sets (A) the heatmap of 29 immune-related gene sets ssGSEA score; (B–D). The violin diagram of difference between immunity-H, -M and -L subtypes of gastric cancer in stroma score (A), immune score (B), total ESTIMATE score (C) and tumor purity (D).

41%; immunity-H, 30%). There was no significant difference in the distributions of gender and race among the three immune subtypes (Supplementary Figure S1B,C).

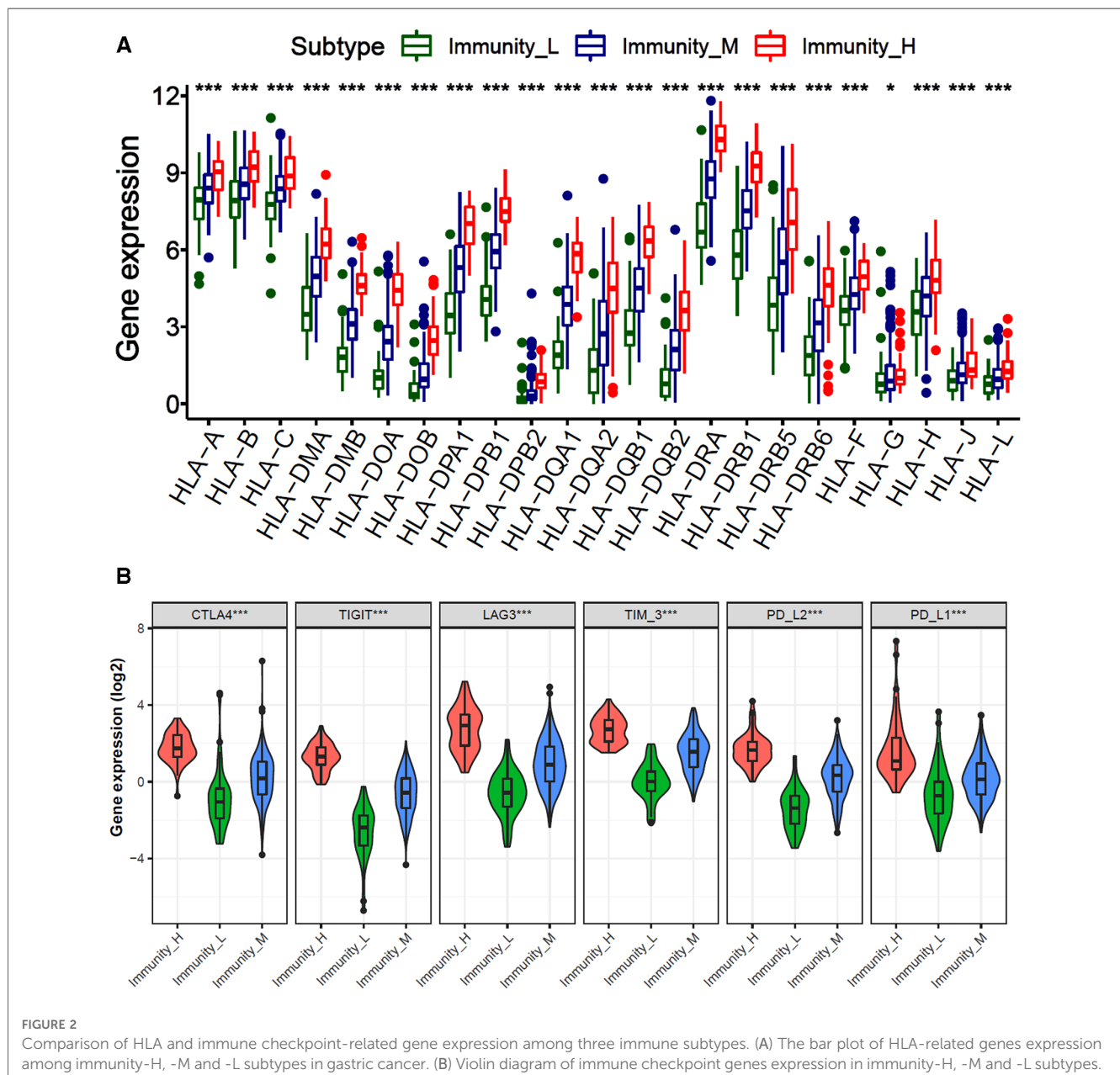
### 3.3. Comparison of immune checkpoint and HLA-related genes expression among three immune subtypes

To explore the expression of immune-related genes among different immune subtypes of gastric cancer, we analyzed the expression of human leukocyte-associated antigen (HLA) genes and immune checkpoint genes. The results showed that the levels of all HLA genes were the highest expressed in the immunity-H subtype and the lowest in the immunity-L subtype ( $P < 0.001$ )

(Figure 2A). Moreover, the expression of immune checkpoint molecules, such as CTLA4, TIGIT, LAG3, TIM-3, PD-L2, and PD-L1 are also the highest in the immunity-H subtype and the lowest in the immunity-L subtype (Figure 2B). These results indicate that the immune subtypes of GC are significantly correlated with the expression of immune-related genes.

### 3.4. Function enrichment analysis of differentially expressed genes and identification of prognostic-related core genes

A total of 1226 differentially expressed genes were identified between immunity-H and -L subtypes, and are presented with



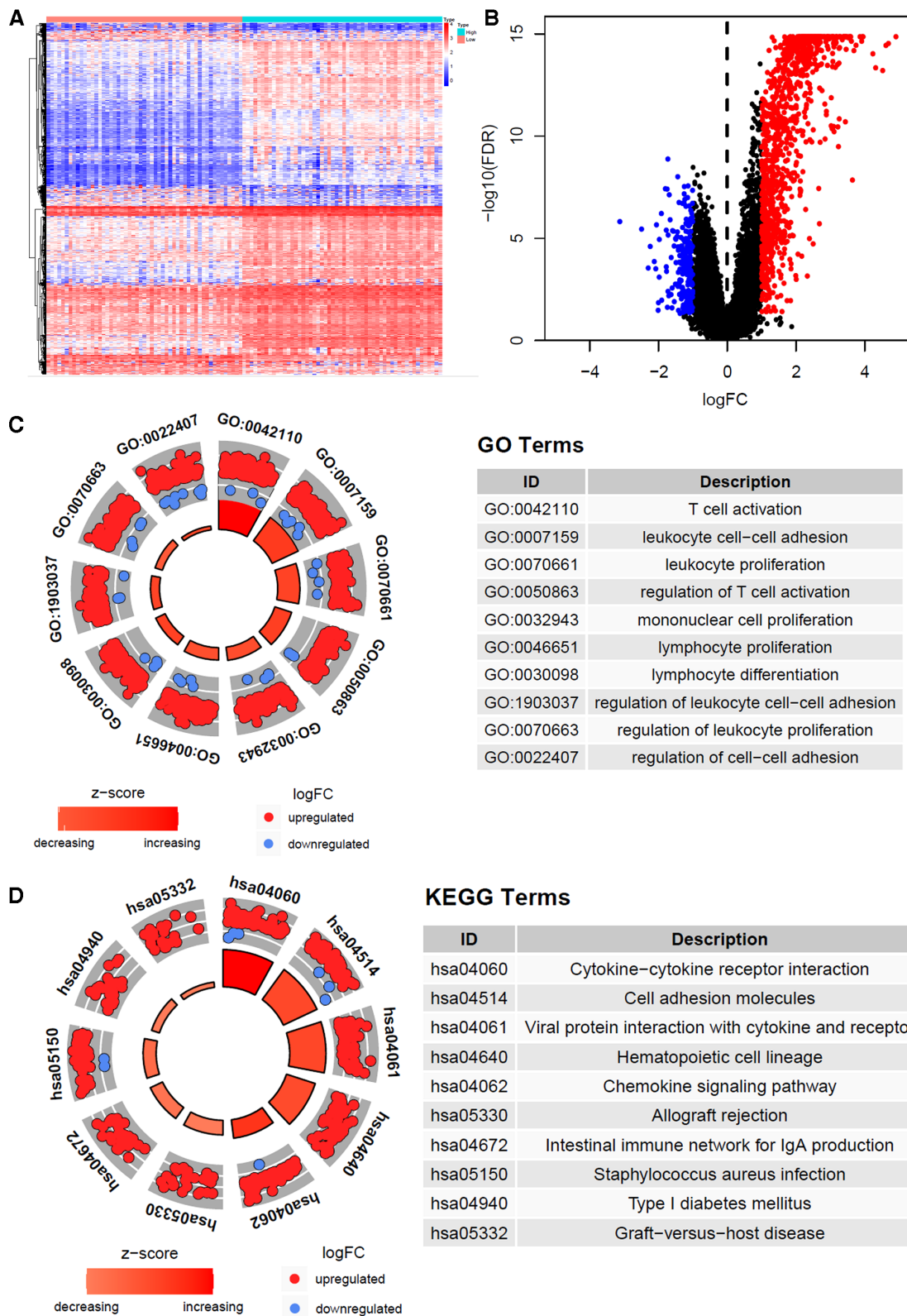


**FIGURE 3** Gene expression heatmap, volcano map and function enrichment analysis of differentially expressed genes. (A) The heat map of differentially expressed genes of high and low immune subtypes in gastric cancer ( $|\log FC| > 1, P < 0.05$ ). (B) Volcano map of differentially expressed genes. (C) Differentially expressed genes Circle diagram of GO and KEGG pathway enrichment analysis.

heatmap (Figure 3A) as well as volcano map (Figure 3B). The GO enrichment analysis showed that immune-related pathways such as T cell activation, lymphocyte differentiation, lymphocyte proliferation, cytokine and cytokine receptor interaction and chemokine signaling pathway were significantly enriched in the immunity-H subtype. These results also support the higher immune activity of immunity-H GC subtype.

### 3.5. Construction and validation of prognosis signature based on immune microenvironment for gastric cancer

We randomly divided the 350 GC patients into training ( $n = 246$ ) and testing ( $n = 104$ ) cohorts. The distribution of baseline data was balanced in training and testing cohorts (Table 2). In the TCGA training cohort, we first identified 1,266 differentially expressed genes between immune-H and -L subtypes, and further

screened out 90 prognosis-related genes via univariate Cox regression ( $P < 0.05$ ). Next, we used lasso-Cox regression to remove the collinearity among genes (Figures 4A,B), and screened out 14 prognostic-related genes, including 3 protective genes and 11 risk genes (Figure 4C). Finally, we identified 7 prognosis-related hub genes by multivariate Cox “stepwise regression” method (Figure 4D).

Based on the expression level and regression coefficients of the seven core genes, the formula of IMPS was shown in the Methods section. Using the median IMPS of 1.07 as the cut-off value for the prognostic risk of gastric cancer, the patients were divided into the high- and low-IMPS groups (Figure 5A). Next, we observed that the proportion of death gradually increased and the survival time gradually decreased as IMPS score increased (Figure 5D), which indicated that the IMPS was closely related to the prognostic risk of GC in the real world. We further explored the association between IMPS and the 7 prognostic hub gene expression. The expression heatmap showed that the expression of VWF and

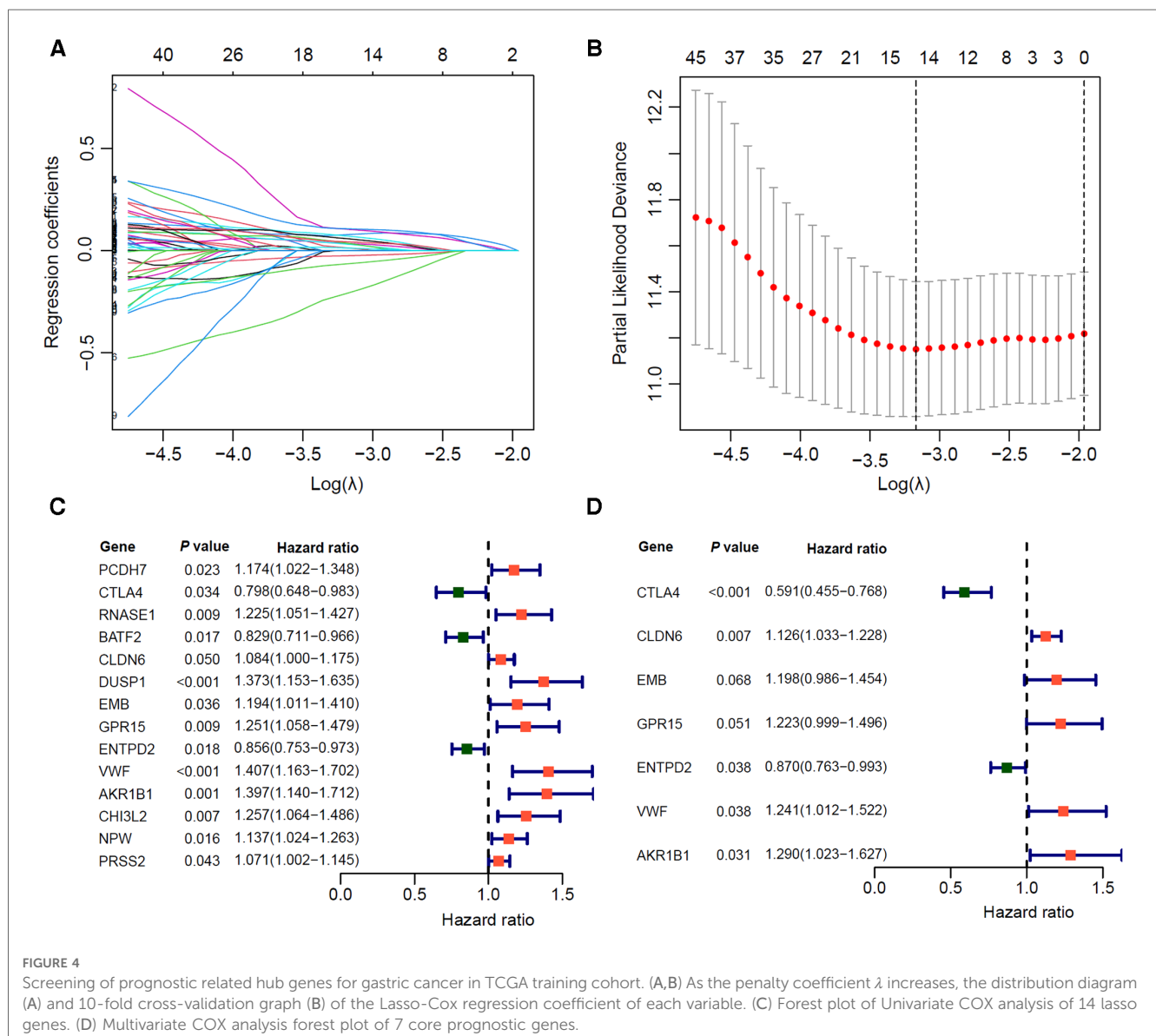


TABLE 2 Distribution of clinical baseline data of gastric cancer patients in training and testing cohorts.

Variables	Overall	Training cohort	Testing cohort	<i>P</i>
	350	246	104	
Age (%)				0.111
<60	106 (30.3)	82 (33.3)	24 (23.1)	
60–69	106 (30.3)	68 (27.6)	38 (36.5)	
70–79	117 (33.4)	79 (32.1)	38 (36.5)	
>80	21 (6.0)	17 (6.9)	4 (3.8)	
Gender (%)				0.873
Male	226 (64.6)	160 (65.0)	66 (63.5)	
Female	124 (35.4)	86 (35.0)	38 (36.5)	
Origin (%)				0.218
Body	84 (24.0)	56 (22.8)	28 (26.9)	
Cardia	86 (24.6)	66 (26.8)	20 (19.2)	
Fundus	40 (11.4)	23 (9.3)	17 (16.3)	
Gastric antrum	127 (36.3)	91 (37.0)	36 (34.6)	
Other	13 (3.7)	10 (4.1)	3 (2.9)	
Grade (%)				0.426
G1	9 (2.6)	7 (2.8)	2 (1.9)	
G2	125 (35.7)	83 (33.7)	42 (40.4)	
G3	207 (59.1)	148 (60.2)	59 (56.7)	
GX	9 (2.6)	8 (3.3)	1 (1.0)	
TNM_stage (%)				0.202
NA	14 (4.0)	10 (4.1)	4 (3.8)	
stage I	46 (13.1)	29 (11.8)	17 (16.3)	
stage II	110 (31.4)	76 (30.9)	34 (32.7)	
stage III	143 (40.9)	99 (40.2)	44 (42.3)	
stage IV	37 (10.6)	32 (13.0)	5 (4.8)	
T_stage (%)				0.369
T1	16 (4.6)	9 (3.7)	7 (6.7)	
T2	74 (21.1)	48 (19.5)	26 (25.0)	
T3	161 (46.0)	118 (48.0)	43 (41.3)	
T4	95 (27.1)	69 (28.0)	26 (25.0)	
TX	4 (1.1)	2 (0.8)	2 (1.9)	
N_stage (%)				0.139
N0	103 (29.4)	64 (26.0)	39 (37.5)	
N1	93 (26.6)	73 (29.7)	20 (19.2)	
N2	72 (20.6)	53 (21.5)	19 (18.3)	
N3	71 (20.3)	49 (19.9)	22 (21.2)	
NX	11 (3.1)	7 (2.8)	4 (3.8)	
M_stage (%)				0.138
M0	312 (89.1)	214 (87.0)	98 (94.2)	
M1	25 (7.1)	21 (8.5)	4 (3.8)	
MX	13 (3.7)	11 (4.5)	2 (2.0)	

NA, not available.

AKR1B1 was positively correlated with IMPS (Figure 5G). Similar phenomena were also observed in the test set and the GEO independent validation set (testing cohort: Figures 5B,E,H; GSE15459 cohort: Figures 5C,F,I). In addition, the GC patients in the high-IMPS group had poorer survival in the training cohort than the low-IMPS group (Figure 5J;  $P < 0.001$ ), with consistent conclusions in the testing cohort (Figures 5K,L; both with  $P < 0.01$ ). To reduce bias, we further validated our model in GSE62254 (Supplementary Figure S2A), GSE57330 (Supplementary Figure S2B) and GSE34942 (Supplementary Figure S2C) independent cohorts. We explored the predictive value of IMPS in the outcome of immunotherapy response in

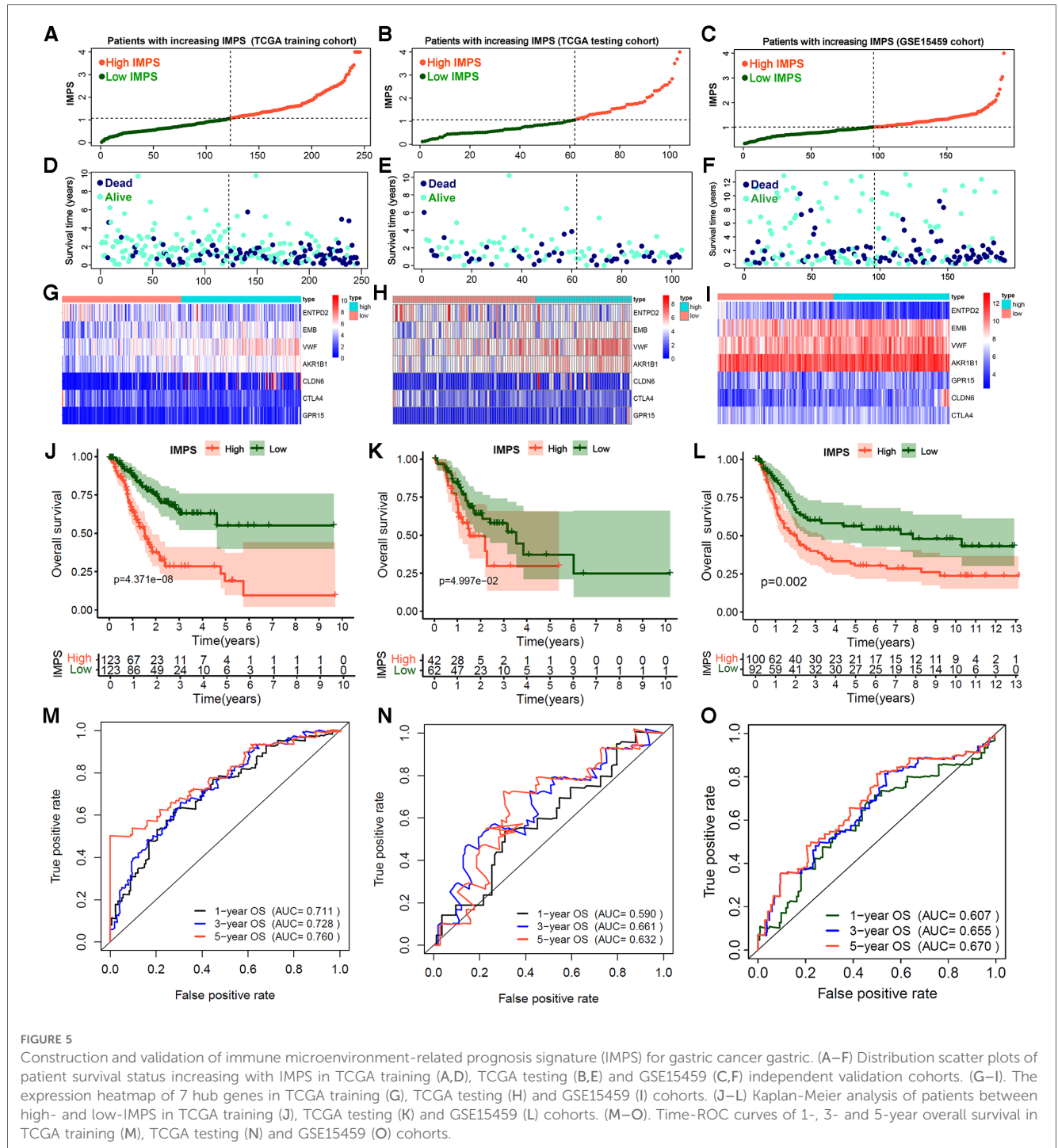
IMvigor210 and Riaz-2017 cohorts. The patients in low-IMPS subgroup have a better OS rate and higher response fraction than the high-IMPS subgroup (Supplementary Figures S2C–F).

Finally, we evaluated the accuracy of the IMPS in predicting 1-year, 3-year and 5-year OS of GC by the survival ROC curve. The prediction accuracy AUCs in the training cohort were 0.711, 0.728 and 0.760, respectively; in the testing cohort 0.590, 0.661 and 0.632, respectively; and in the GSE15459 cohort 0.607, 0.655 and 0.670, respectively. Furthermore, the multivariate Cox analysis showed that the IMPS was an independent risk factor for GC prognostic after adjustment by age, gender, grade and TNM stage (Table 3,  $P < 0.001$ ). These findings suggest that the IMPS we identified has moderate predictive value in GC prognostic risk assessment.

To further explore the prognosis value of 7 hub genes, we performed Kaplan-Meier curve survival analysis in the TCGA-STAD, GSE15459 and GSE57303 cohorts. The results showed that patients in the TCGA-STAD cohort with high expression of CTLA4 and ENTPD2 had a better OS (Figures 6A–C, both  $P < 0.05$ ), whereas patients with high expression of EMB, GPR15, CLDN6, VWF and AKR1B1 had a poorer OS (Figures 6D–I, all  $P < 0.05$ ). These findings were further confirmed in GSE15459 and GSE57303 cohorts (Supplementary Figures S3A–N). In addition, we performed RT-PCR to explore the differential expressions between human GC (MKN45 and AGS) and normal gastric mucosal epithelial cell lines (GES-1). The RT-PCR results showed that the CTLA4 and ENTPD2 were highly expressed in normal gastric mucosal epithelial cell lines (GES-1), while the EMB, CLDN6, VWF and AKR1B1 were highly expressed in human GC cell lines (MKN45 and AGS), and the expression of GPR15 had no significant difference between normal and tumor cell lines (Supplementary Figure S4A). We further performed the PCR verification of seven Hub genes in five paired benign and tumor gastric tissue samples. Compared with benign tissues, the CTLA4 and ENTPD2 were highly expressed in gastric tumor tissues, while the AKR1B1, CLDN6, EMB, GPR15 and VWF were highly expressed (Supplementary Figures S4B,C).

### 3.7. Correlation analysis of IMPS with clinical characteristics and somatic mutations

The alluvial diagram of the immunity subtypes with different pathological grades, TNM stages and IMPS subgroups (Figure 7A) indicated that the immunity-H subtype was more likely linked to the higher grade, more advanced TNM stages and higher IMPS; while the immunity-L subtype exhibited a lower grade, earlier TNM stages and lower IMPS. The GC patients in immunity-M subtype showed higher IMPS than those in immunity-L and immunity-H subtypes (Figure 7B,  $P = 0.016$  and  $P = 0.063$ ). GC patients with higher IMPS were also more likely to be associated with higher grade, more advanced TNM stages, higher T and N stage, and death (Figures 7C–F, all  $P < 0.001$ ). The mutation landscape showed that the patients in the IMPS-H subtype had a higher mutation alter ratio (81.25%) than



the IMPS-L subtype (93.96%) with higher tumor mutation burden (Figure 7H).

### 3.8. Construction and evaluation of the combined nomogram considering IMPS and clinical characteristics

In order to enhance the prediction performance, we further constructed a combined nomogram considering IMPS and

clinical characteristics (Figure 8). The nomogram showed that patient with higher TNM stage, older age and higher IMPS was significantly correlated with poorer prognosis. We further performed the calibration curve and time-ROC curve to present the consistency and prediction value of the combined nomogram with the actual observed OS of 1, 3, and 5 years. The calibration curve exhibited high consistency of OS prediction with the actual observation (Figure 9A).

The combined nomogram (AUC = 0.750) showed the highest value of the 1-year OS prediction (Figure 9B), followed by IMPS

TABLE 3 Multivariate Cox analysis of IMPS and clinical features for gastric cancer prognosis.

Variables	HR	HR (95% CI)	P-value
<b>IMPS (Low)</b>	Ref.		
High	2.88	4.14–2.00	<0.001
<b>Age (&lt;60)</b>	Ref.		
60–69	1.65	1.03–2.62	0.037
70–79	2.25	1.45–3.50	<0.001
>80	2.34	0.96–5.69	0.061
<b>Gender (Female)</b>	Ref.		
Male	1.33	0.92–1.91	0.128
<b>Grade (G1)</b>	Ref.		
G2	2.96	0.40–21.73	0.286
G3	4.01	0.56–29.85	0.164
<b>TNM (Stage I)</b>	Ref.		
Stage II	1.26	0.64–2.46	0.502
Stage III	1.94	1.03–3.64	0.039
Stage IV	3.09	1.49–6.39	0.003

HR, hazard rate; CI, confidence interval.

(AUC = 0.669), TNM stage (AUC = 0.607), age (AUC = 0.580), grade (AUC = 0.567) and gender (AUC = 0.529). The AUC values of the combined nomogram in predicting 3-year (AUC = 0.764) and 5-year (AUC = 0.802) OS were also higher than those with IMPS and individual clinical characteristics (Figures 9C,D). These results indicate that the combined nomogram model is more accurate than IMPS and the individual clinical characteristics of TNM stage, age, grade and gender in predicting the OS of GC patients.

### 4. Discussion

In recent years, the GC classification based on multi-omics analysis has been extensively studied, and these efforts may lay the foundation for the development of novel GC biomarkers and drug targets (24–26). It has also been demonstrated that the

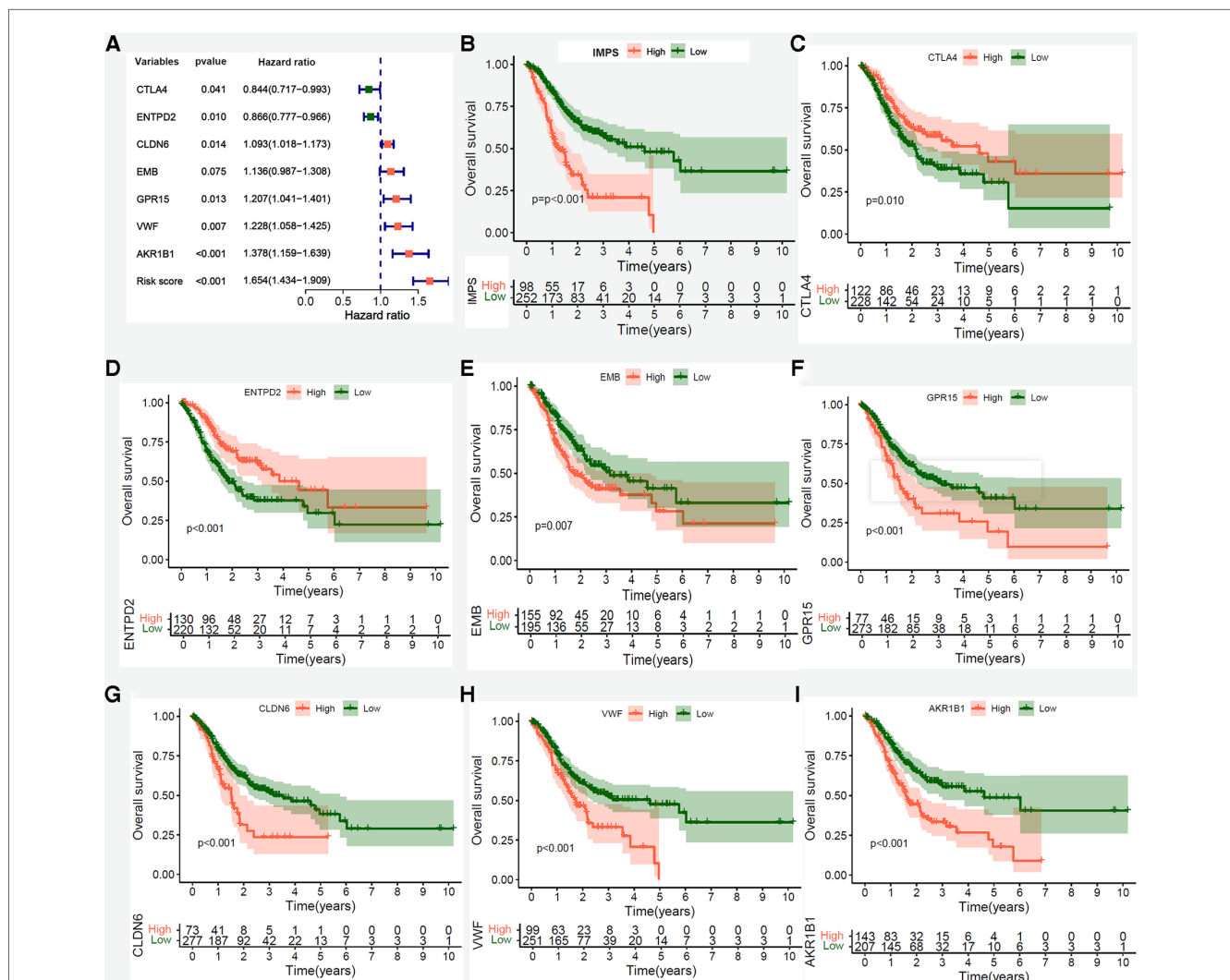
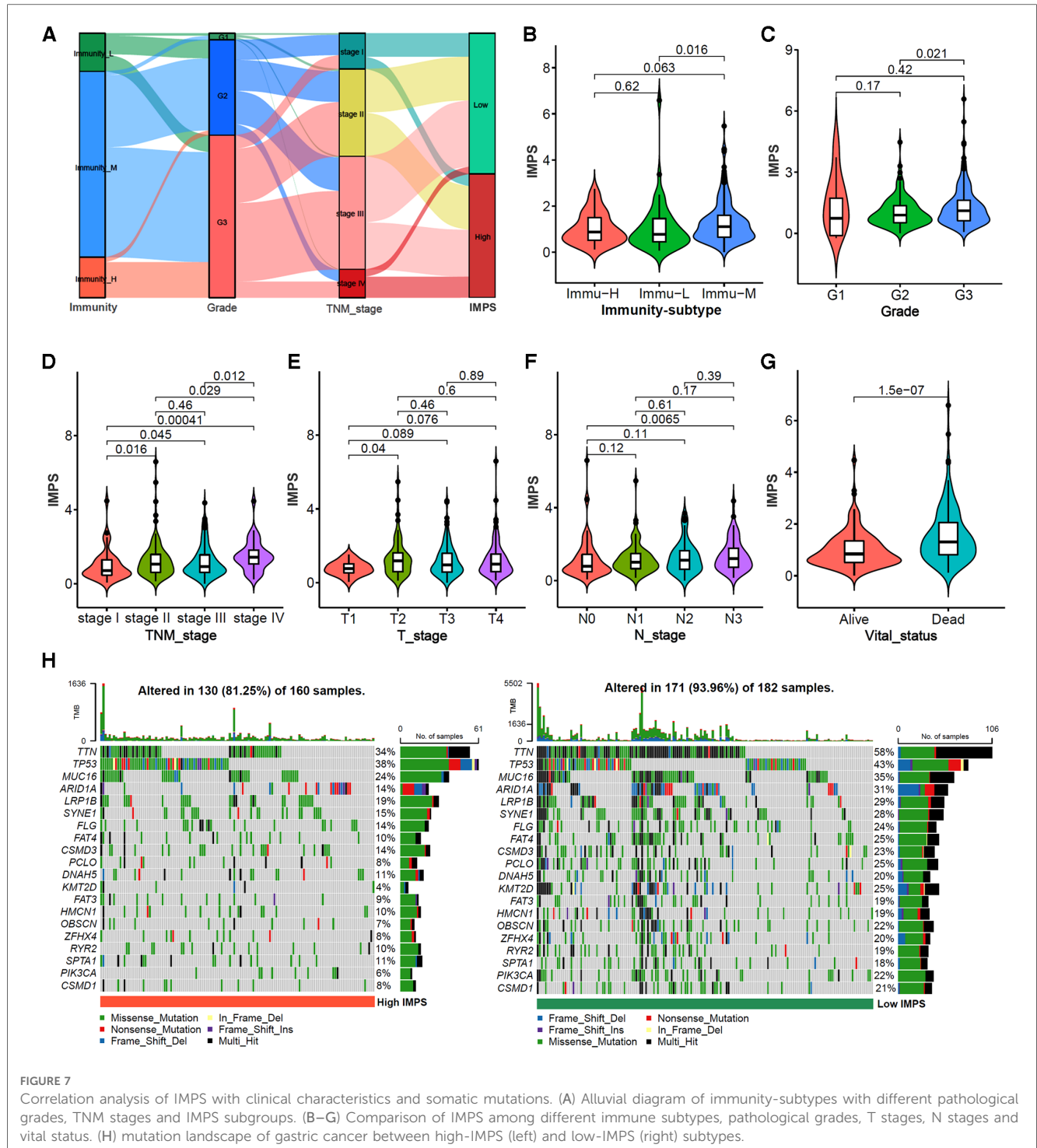


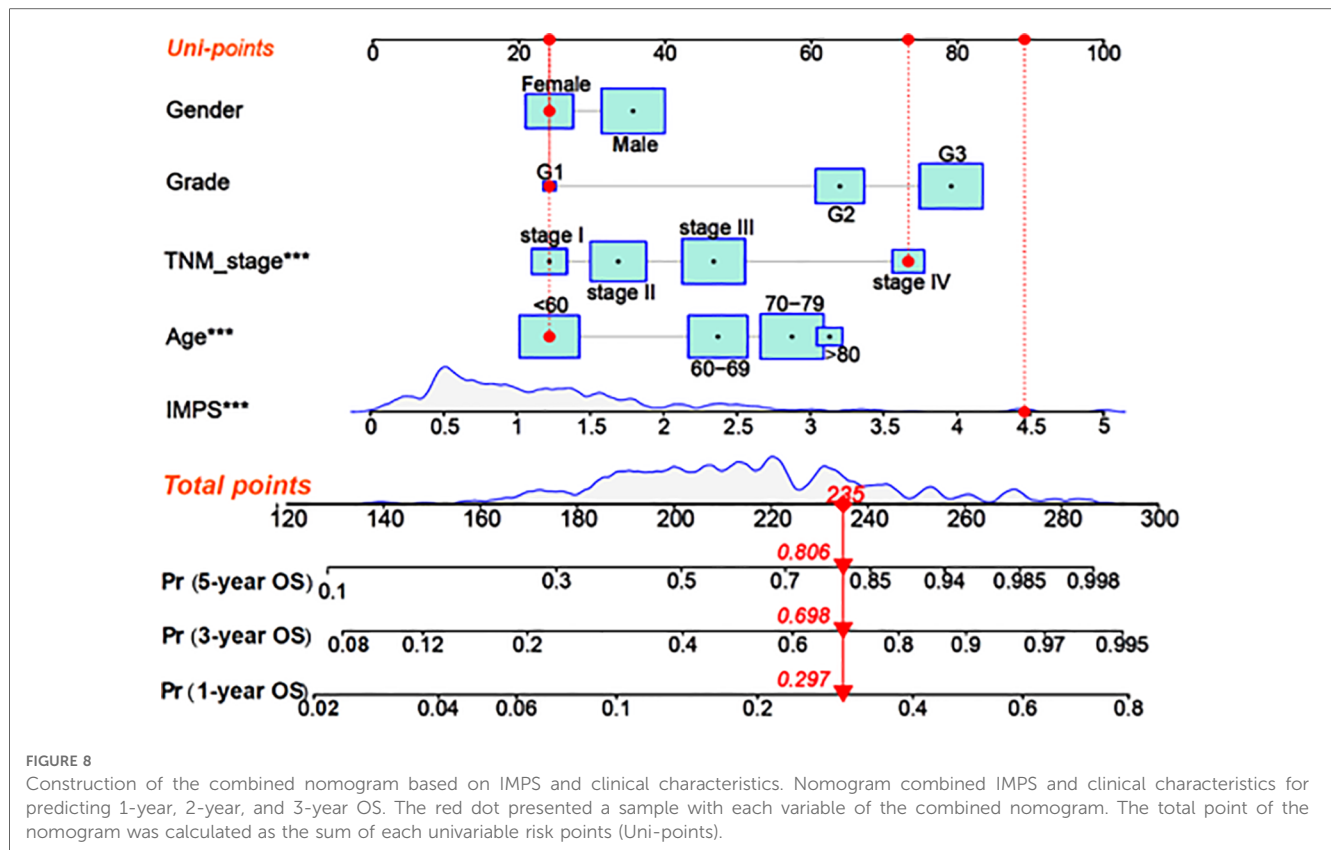
FIGURE 6 Kaplan-Meier survival analysis of IMPS and 7 prognostic hub genes in the entire TCGA-STAD cohort. (A) Univariate Cox forest-plot of IMPS and 7 prognostic hub genes. (B–G) Kaplan-Meier curve survival analysis of IMPS and 7 core prognostic gene, red line means high expression group, blue line means low expression group. (B) IMPS, (C) CTLA4, (D) ENTPD2, (E) EMB, (F)GPR15, (G) CLDN6, (H) VWF and (I) AKR1B1.



TME components play a crucial role in tumor development. However, the tumor-immune interactions have not been fully understood. In the present study, we identified three immunophenotypes (immunity-H, -M and -L) based on the characteristics of 29 immune-related gene sets. In addition, we constructed an immune microenvironment-related prognosis signature (IMPS) *via* univariate Cox regression, Lasso-Cox regression, and multivariate Cox regression, and validated in the testing and independent cohorts. The patients with higher IMPS

were associated with higher grade, advanced TNM stages, higher T and N stage, and death. We further constructed a nomogram model combining IMPS and clinical variables. The IMPS and the combined nomogram model have potential value in predicting survival outcomes of gastric cancer.

We further constructed a 7-gene (CTLA4, CLDN6, EMB, GPR15, ENTPD2, VWF and AKR1B1) prognosis signature, IMPS, based on the immune microenvironment and screened by univariate Cox regression, Lasso-Cox regression, and multivariate

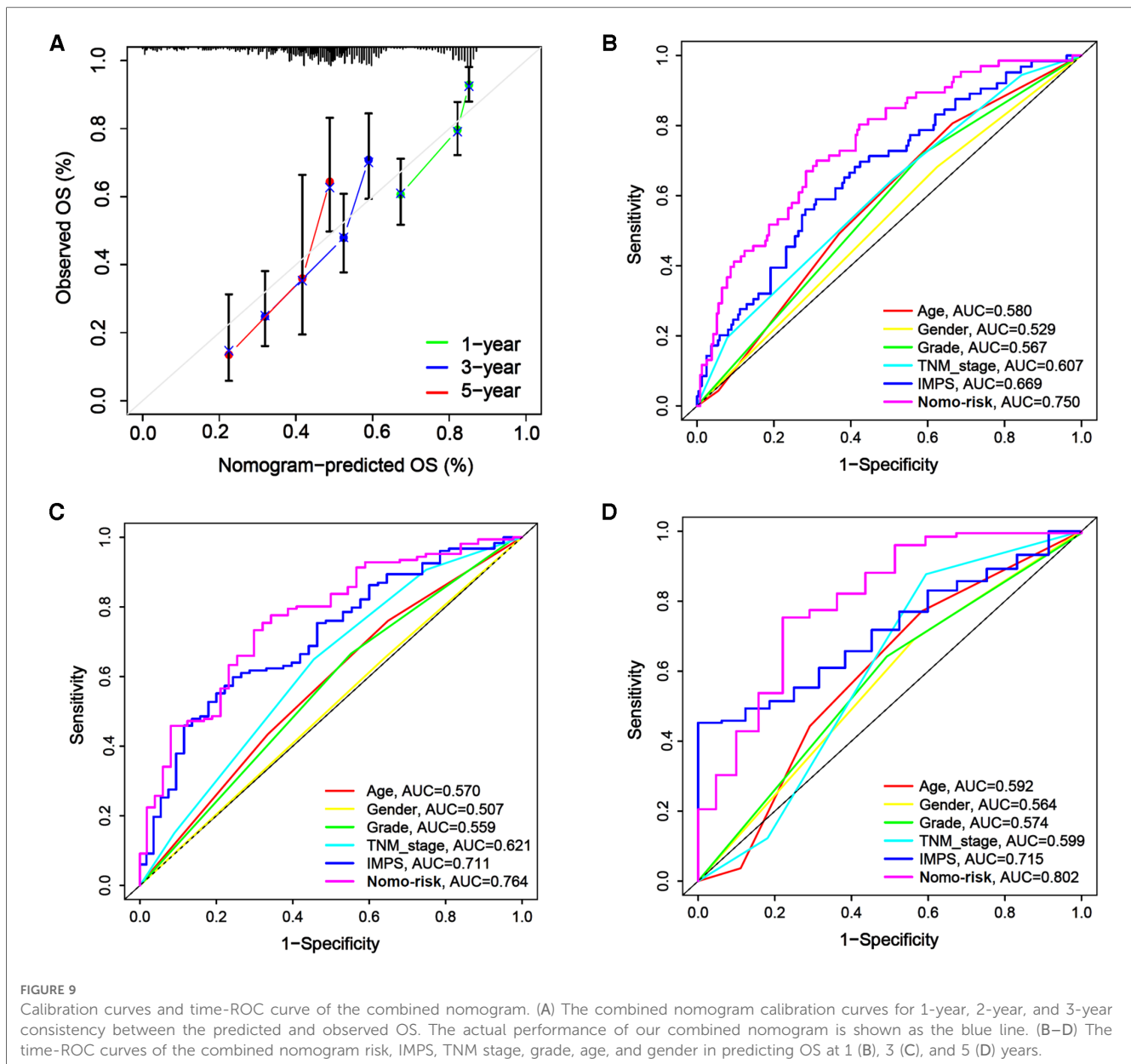


Cox regression. In this study, the gastric cancer patients with high expression of CTLA4 and ENTPD2 had a better survival prognosis, with high expression of CLDN6, EMB, GPR15, VWF and AKR1B1 suggesting poor prognosis, which was consistent with previous studies. CTLA4 is an immune checkpoint gene, and drugs of CTLA4 inhibitors have been used in clinical practice (27, 28). In addition, CTLA4 is mainly expressed in the T cells' cytoplasm, and its membrane levels are changing dynamically during T cell activation (29). By inhibiting the expression of CTLA4 in tumors, it can increase the antigen presentation of CD4<sup>+</sup> T cells, and improve the killing effect of CD8<sup>+</sup> T cells on tumors. Patients with high CTLA4 expression potentially benefit from treatment with CTLA4 inhibitors (30). Overexpression of nucleoside triphosphate diphosphate hydrolase 2 (ENTPD2) is an indicator of poor prognosis in HCC, Chiu DK et al. found that in HCC, ENTPD2 converts extracellular ATP into 5'-AMP, prevents myeloid-derived suppressor cells (MDSC) differentiation, promotes MDSC maintenance (31), and allows HCC cells to escape immune surveillance (32), but it has not been reported in gastric cancer. In this study, we found that elevated ENTPD2 expression suggests better overall survival, which may be related to cancer type differences and internal heterogeneity of tumors.

Claudin6 (CLDN6) is a member of the tight junction family and is involved in intercellular adhesion (33). Yu S et al. found that CLDN6 can affect EMT process by affecting YAP1 and YAP1-snail1 axis, and promote gastric cancer proliferation and invasion (34). Embigin (EMB), a transmembrane glycoprotein of

the immunoglobulin superfamily (35), is involved in the occurrence and development of prostate cancer, pancreatic cancer and breast cancer, and is associated with poor prognosis in cancer patients (36–38), but not in reports of gastric cancer. G protein-coupled receptor 15 (GPR15) is an unconventional chemokine receptor that mediates T<sub>reg</sub> homing and immunosuppression (39) by directing T<sub>reg</sub> into the colon, thereby altering the tumor microenvironment and promoting occurrence of intestinal tumors (40). Von Willebrand factor (VWF) is a potent regulator of angiogenesis, tumor growth, and metastasis, and gastric cancer-related plasma VWF activity levels are significantly elevated in advanced disease stages (41). Aldehyde-ketoreductase family 1 member B1 (AKR1B1) is overexpressed in a variety of tumors and is involved in inflammation, cell cycle, epithelial-to-mesenchymal transition, cell survival, and apoptosis (42). In GC, the expression of AKR1B1 is significantly correlated with the clinicopathological characteristics, and the patients with low AKR1B1 have a better OS than that in patients with high AKR1B1 (43).

We constructed an immune microenvironment-related prognosis signature (IMPS) in the training cohort, and further validated it in the testing and independent cohorts. The GC patients with higher IMPS were associated with higher TNM stages and had a bad prognosis. And the reliability of IMPS was validated in the TCGA testing and three independent GEO cohorts. We further a nomogram combined with age, gender, pathology grade and TNM stage. The combined nomogram showed best performance in OS time prediction outperforms



IMPS and the individual clinical parameters. The IMPS and the combined nomogram model have potential value in predicting survival outcomes of gastric cancer. Although we collected multiple datasets and conducted comprehensive analyses, this study still needs to be validated by prospective clinical studies with large samples.

## 5. Conclusions

In summary, our study constructed a prognostic signature (IMPS) based on the immune microenvironment, and further constructed a combined nomogram based on IMPS and clinical characteristics. The IMPS and the combined nomogram were well-performed in predicting the 1-, 2- and 5-year overall

survival prognosis, and might provide important value for the diagnosis and treatment of gastric cancer.

## Data availability statement

The original contributions presented in the study are included in the article/[Supplementary Material](#), further inquiries can be directed to the corresponding author.

## Author contributions

JW and XY designed the study and contributed to study materials and consumables. L-HW, X-XW, XY and JW

conducted the study. L-HW, X-XW, YW, JW and Z-RL collected the data. X-XW and L-HW performed the statistical analyses and interpreted the data. L-HW and X-XW wrote the manuscript. All authors contributed to the article and approved the submitted version.

## Conflict of interest

The authors declare that the research was conducted in the absence of any commercial or financial relationships that could be construed as a potential conflict of interest.

## References

- Sexton RE, Hallak M, Uddin MH, Diab M, Azmi AS. Gastric cancer heterogeneity and clinical outcomes. *Technol Cancer Res Treat.* (2020) 19:1079203125. doi: 10.1177/1533033820935477
- Sung H, Ferlay J, Siegel RL, Laversanne M, Soerjomataram I, Jemal A, et al. Global cancer statistics 2020: GLOBOCAN estimates of incidence and mortality worldwide for 36 cancers in 185 countries. *Ca Cancer J Clin.* (2021) 71:209–49. doi: 10.3322/caac.21660
- Smyth EC, Verheij M, Allum W, Cunningham D, Cervantes A, Arnold D. Gastric cancer: ESMO clinical practice guidelines for diagnosis, treatment and follow-up. *Ann Oncol.* (2016) 27:v38–v49. doi: 10.1093/annonc/mdw350
- Taube JM, Galon J, Sholl LM, Rodig SJ, Cottrell TR, Giraldo NA, et al. Implications of the tumor immune microenvironment for staging and therapeutics. *Mod Pathol.* (2018) 31:214–34. doi: 10.1038/modpathol.2017.156
- Cesano A, Warren S. Bringing the next generation of immuno-oncology biomarkers to the clinic. *Biomedicine.* (2018) 6. doi: 10.3390/biomedicine6010014
- Finotello F, Trajanoski Z. Quantifying tumor-infiltrating immune cells from transcriptomics data. *Cancer Immunol Immunother.* (2018) 67:1031–40. doi: 10.1007/s00262-018-2150-z
- Hanzelmann S, Castelo R, Guinney J. GSEA: gene set variation analysis for microarray and RNA-seq data. *Bmc Bioinformatics.* (2013) 14:7. doi: 10.1186/1471-2105-14-7
- Guo J, Li W, Cheng L, Gao X. Identification and validation of hub genes with poor prognosis in hepatocellular carcinoma by integrated bioinformatical analysis. *Int J Gen Med.* (2022) 15:3933–41. doi: 10.2147/IJGM.S353708
- Jin Y, Wang Z, He D, Zhu Y, Chen X, Cao K. Identification of novel subtypes based on ssGSEA in immune-related prognostic signature for tongue squamous cell carcinoma. *Cancer Med.* (2021) 10:8693–707. doi: 10.1002/cam4.4341
- Wang XX, Wu LH, Dou QY, Ai L, Lu Y, Deng SZ, et al. Construction of m6A-based prognosis signature and prediction for immune and anti-angiogenic response. *Front Mol Biosci.* (2022) 9:1034928. doi: 10.3389/fmolb.2022.1034928
- Yoshihara K, Shahmoradgoli M, Martinez E, Vegesna R, Kim H, Torres-Garcia W, et al. Inferring tumour purity and stromal and immune cell admixture from expression data. *Nat Commun.* (2013) 4:2612. doi: 10.1038/ncomms3612
- Newman AM, Liu CL, Green MR, Gentles AJ, Feng W, Xu Y, et al. Robust enumeration of cell subsets from tissue expression profiles. *Nat Methods.* (2015) 12:453–7. doi: 10.1038/nmeth.3337
- Yao F, Zhao C, Zhong F, Qin T, Li S, Liu J, et al. Bioinformatics analysis and identification of hub genes and immune-related molecular mechanisms in chronic myeloid leukemia. *PeerJ.* (2022) 10:e12616. doi: 10.7717/peerj.12616
- Jiang L, Zhu X, Yang H, Chen T, Lv K. Bioinformatics analysis discovers microtubular tubulin beta 6 class V (TUBB6) as a potential therapeutic target in glioblastoma. *Front Genet.* (2020) 11:566579. doi: 10.3389/fgene.2020.566579
- Zhang Z, Li J, Lu K, Wu W, Huang Z, Zhang C, et al. Identification of prognostic markers of N6-methyladenosine-related noncoding RNAs in non-small-cell lung cancer. *J Oncol.* (2022) 2022:3657349. doi: 10.1155/2022/3657349
- Jiang W, Xie N, Xu C. Characterization of a prognostic model for lung squamous cell carcinoma based on eight stemness index-related genes. *Bmc Pulm Med.* (2022) 22:224. doi: 10.1186/s12890-022-02011-0

## Publisher's note

All claims expressed in this article are solely those of the authors and do not necessarily represent those of their affiliated organizations, or those of the publisher, the editors and the reviewers. Any product that may be evaluated in this article, or claim that may be made by its manufacturer, is not guaranteed or endorsed by the publisher.

## Supplementary material

The Supplementary Material for this article can be found online at: <https://www.frontiersin.org/articles/10.3389/fsurg.2023.1088292/full#supplementary-material>.

- Xing M, Li J. Diagnostic and prognostic values of pyroptosis-related genes for the hepatocellular carcinoma. *Bmc Bioinformatics.* (2022) 23:177. doi: 10.1186/s12859-022-04726-7
- Mariathanas S, Turley SJ, Nickles D, Castiglioni A, Yuen K, Wang Y, et al. TGFbeta attenuates tumour response to PD-L1 blockade by contributing to exclusion of T cells. *Nature.* (2018) 554:544–8. doi: 10.1038/nature25501
- Riaz N, Havel JJ, Makarov V, Desrichard A, Urba WJ, Sims JS, et al. Tumor and microenvironment evolution during immunotherapy with nivolumab. *Cell.* (2017) 171:934–49. doi: 10.1016/j.cell.2017.09.028
- Zhu J, Ao H, Liu M, Cao K, Ma J. UBE2T Promotes autophagy via the p53/AMPK/mTOR signaling pathway in lung adenocarcinoma. *J Transl Med.* (2021) 19:374. doi: 10.1186/s12967-021-03056-1
- Wang XX, Wu LH, Ai L, Pan W, Ren JY, Zhang Q, et al. Construction of an HCC recurrence model based on the investigation of immune-related lncRNAs and related mechanisms. *Mol Ther Nucleic Acids.* (2021) 26:1387–400. doi: 10.1016/j.omtn.2021.11.006
- Zhang T, Zhu L, Cai J, He J. Four drug metabolism-related subgroups of pancreatic adenocarcinoma in prognosis, immune infiltration, and gene mutation. *Open Med (Wars).* (2022) 17:427–40. doi: 10.1515/med-2022-0433
- Zou X, Wei Y, Qi T, Wang X, Zuo W, Wang T, et al. A novel 6-gene signature derived from tumor-infiltrating T cells and neutrophils predicts survival of bladder urothelial carcinoma. *Aging (Albany NY).* (2021) 13:25496–517. doi: 10.18632/aging.203770
- Serra O, Galan M, Ginesta MM, Calvo M, Sala N, Salazar R. Comparison and applicability of molecular classifications for gastric cancer. *Cancer Treat Rev.* (2019) 77:29–34. doi: 10.1016/j.ctrv.2019.05.005
- Bijlsma MF, Sadanandam A, Tan P, Vermeulen L. Molecular subtypes in cancers of the gastrointestinal tract. *Nat Rev Gastroenterol Hepatol.* (2017) 14:333–42. doi: 10.1038/nrgastro.2017.33
- Russi S, Marano L, Laurino S, Calice G, Scala D, Marino G, et al. Gene regulatory network characterization of gastric cancer's histological subtypes: distinctive biological and clinically relevant master regulators. *Cancers (Basel).* (2022) 14(19):4961. doi: 10.3390/cancers14194961
- Schlosser HA, Drebber U, Kloth M, Thelen M, Rothschild SI, Haase S, et al. Immune checkpoints programmed death 1 ligand 1 and cytotoxic T lymphocyte associated molecule 4 in gastric adenocarcinoma. *Oncimmunology.* (2016) 5: e1100789. doi: 10.1080/2162402X.2015.1100789
- Chang X, Lu X, Guo J, Teng GJ. Interventional therapy combined with immune checkpoint inhibitors: emerging opportunities for cancer treatment in the era of immunotherapy. *Cancer Treat Rev.* (2019) 74:49–60. doi: 10.1016/j.ctrv.2018.08.006
- Van Coillie S, Wiernicki B, Xu J. Molecular and cellular functions of CTLA-4. *Adv Exp Med Biol.* (2020) 1248:7–32. doi: 10.1007/978-981-15-3266-5\_2
- Teft WA, Kirchhof MG, Madrenas J. A molecular perspective of CTLA-4 function. *Annu Rev Immunol.* (2006) 24:65–97. doi: 10.1146/annurev.immunol.24.021605.090535
- Oura K, Morishita A, Tani J, Masaki T. Tumor immune microenvironment and immunosuppressive therapy in hepatocellular carcinoma: a review. *Int J Mol Sci.* (2021) 22(11):5801. doi: 10.3390/ijms22115801
- Vuerich M, Robson SC, Longhi MS. Ectonucleotidases in intestinal and hepatic inflammation. *Front Immunol.* (2019) 10:507. doi: 10.3389/fimmu.2019.00507

33. Lal-Nag M, Morin PJ. The claudins. *Genome Biol.* (2009) 10:235. doi: 10.1186/gb-2009-10-8-235
34. Yu S, Zhang Y, Li Q, Zhang Z, Zhao G, Xu J. CLDN6 Promotes tumor progression through the YAP1-snail1 axis in gastric cancer. *Cell Death Dis.* (2019) 10:949. doi: 10.1038/s41419-019-2168-y
35. Guenette RS, Sridhar S, Herley M, Mooibroek M, Wong P, Tenniswood M. Embigin, a developmentally expressed member of the immunoglobulin super family, is also expressed during regression of prostate and mammary gland. *Dev Genet.* (1997) 21:268–78. doi: 10.1002/(SICI)1520-6408(1997)21:4<268::AID-DVG4>3.0.CO;2-5
36. Chao F, Zhang J, Zhang Y, Liu H, Yang C, Wang J, et al. Embigin, regulated by HOXC8, plays a suppressive role in breast tumorigenesis. *Oncotarget.* (2015) 6:23496–509. doi: 10.18632/oncotarget.4360
37. Ruma I, Kinoshita R, Tomonobu N, Inoue Y, Kondo E, Yamauchi A, et al. Embigin promotes prostate cancer progression by S100A4-dependent and-independent mechanisms. *Cancers (Basel).* (2018) 10(7):239. doi: 10.3390/cancers10070239
38. Jung DE, Kim JM, Kim C, Song SY. Embigin is overexpressed in pancreatic ductal adenocarcinoma and regulates cell motility through epithelial to mesenchymal transition via the TGF-beta pathway. *Mol Carcinog.* (2016) 55:633–45. doi: 10.1002/mc.22309
39. Tindemans I, Joosse ME, Samsom JN. Dissecting the heterogeneity in T-cell mediated inflammation in IBD. *Cells.* (2020) 9(1):110. doi: 10.3390/cells9010110
40. Fischer A, Zundler S, Atreya R, Rath T, Voskens C, Hirschmann S, et al. Differential effects of alpha4beta7 and GPR15 on homing of effector and regulatory T cells from patients with UC to the inflamed gut in vivo. *Gut.* (2016) 65:1642–64. doi: 10.1136/gutjnl-2015-310022
41. Yang X, Sun HJ, Li ZR, Zhang H, Yang WJ, Ni B, et al. Gastric cancer-associated enhancement of von Willebrand factor is regulated by vascular endothelial growth factor and related to disease severity. *Bmc Cancer.* (2015) 15:80. doi: 10.1186/s12885-015-1083-6
42. Khayami R, Hashemi SR, Kerachian MA. Role of aldo-keto reductase family 1 member B1 (AKR1B1) in the cancer process and its therapeutic potential. *J Cell Mol Med.* (2020) 24:8890–902. doi: 10.1111/jcmm.15581
43. Li X, Yang J, Gu X, Xu J, Li H, Qian J, et al. The expression and clinical significance of aldo-keto reductase 1 member B1 in gastric carcinoma. *Dna Cell Biol.* (2020) 39:1322–7. doi: 10.1089/dna.2020.5550